Pergamon

Int. J. Solids Structures Vol. 34, No. 13, pp. 1563–1581, 1997

0020-7683/97 $17.00 + .00

PII: S0020-7683(96)00107-2

# THERMAL SOFTENING OF A PARTICLE-MODIFIED TUNGSTEN-BASED COMPOSITE UNDER ADIABATIC COMPRESSION

P. R. LEDUC and G. BAO
Department of Mechanical Engineering, G.W.C. Whiting School of Engineering, 125 Latrobe Hall, 3400 N. Charles Street, Baltimore, MD 21218–2686, U.S.A.

(*Received* 27 *March* 1996; *in revised form* 4 *June* 1996)

**Abstract**—A micromechanics study is made of the rate-dependent thermal softening behavior of a tungsten matrix composite containing glassy particles. Under adiabatic compression of the composite, the elastic glassy particles thermally soften at relatively high strains, enhancing the thermal softening of the tungsten-based composite, thus reducing the strain rate sensitivity and fostering shear localization. To guide the microstructural design of the particle-modified tungsten-based composite in penetration applications, systematic predictions are made for the stress-strain behavior of the composite under overall adiabatic compression with different temperature-dependent behaviors, sizes, volume fractions of the particle and different applied strain rates. The temperature-dependent behavior of the particles is characterized by a set of exponential functions using two non-dimensional parameters and a reference temperature. The plastic behavior of tungsten is taken to be power-law strain and strain rate hardening. It is found that the radius r of the particles has very little influence on the composite behavior if $r \leqslant 10\ \mu m$. It is also found that both the onset and the rate of thermal softening of the composite depend critically on the applied strain rate. Owing to thermal softening of the glassy particles, the strain-rate sensitivity of the composite is reduced.


## 1. INTRODUCTION

Dual-phase metal alloys such as depleted uranium (DU) and tungsten heavy alloys (WHA) are used or being developed as penetrator materials in advanced anti-armor systems owing to their attractive mechanical properties: high density, high strength and moderate ductility (Magness and Farrand, 1990; Magness, 1992a; German, 1993). Under impact loading conditions, both the penetrator and the armor materials undergo ultra-high-strain-rate plastic deformation (Hohler and Stilp, 1990; Chin *et al.*, 1993; Magness, 1994). High hydrostatic pressure builds up on either side of the penetrator-armor interface. The deformation process is very complex—the heat generated due to plastic work causes thermal softening, perhaps leading to a dramatic change of material behavior within the head of the penetrator (Magness, 1994). As illustrated schematically in Fig. 1, two quite different deformation and failure modes have been observed. A penetrator made of U-3/4 Ti can keep its "nose" sharp during penetration, apparently due to shear localization; this "self-sharpening" mechanism results in a superior ballistic performance (Magness and Farrand, 1990). However, the application of DU as a penetrator material is very expensive, since the material is toxic and thus requires a major clean-up effort, both during manufacturing and after fielding. Considered as a possible alternative to the DU penetrator, WHAs consisting of tungsten particles in a relatively softer matrix have densities and quasistatic strengths similar to the DU alloys (Magness and Farrand, 1990; Magness, 1994). However, their mechanical behavior at high strain rates is known to be different from that of DU (Magness, 1992b; Dunn and Baker, 1993). The tungsten heavy alloy penetrator often forms a "mushroom" head during the penetration process (Fig. 1), resulting in an inefficient dissipation of the kinetic energy and a loss of penetration depth (Magness, 1994).

There is some evidence suggesting that, for DU-alloy penetrators, shear localization dictates the self-sharpening of the penetrator head (Magness, 1994). During penetration, the DU alloy near the penetrator/armor interface undergoes thermal softening under shear; it then fails at relatively small strains, forming "chips" that flow back along the walls of

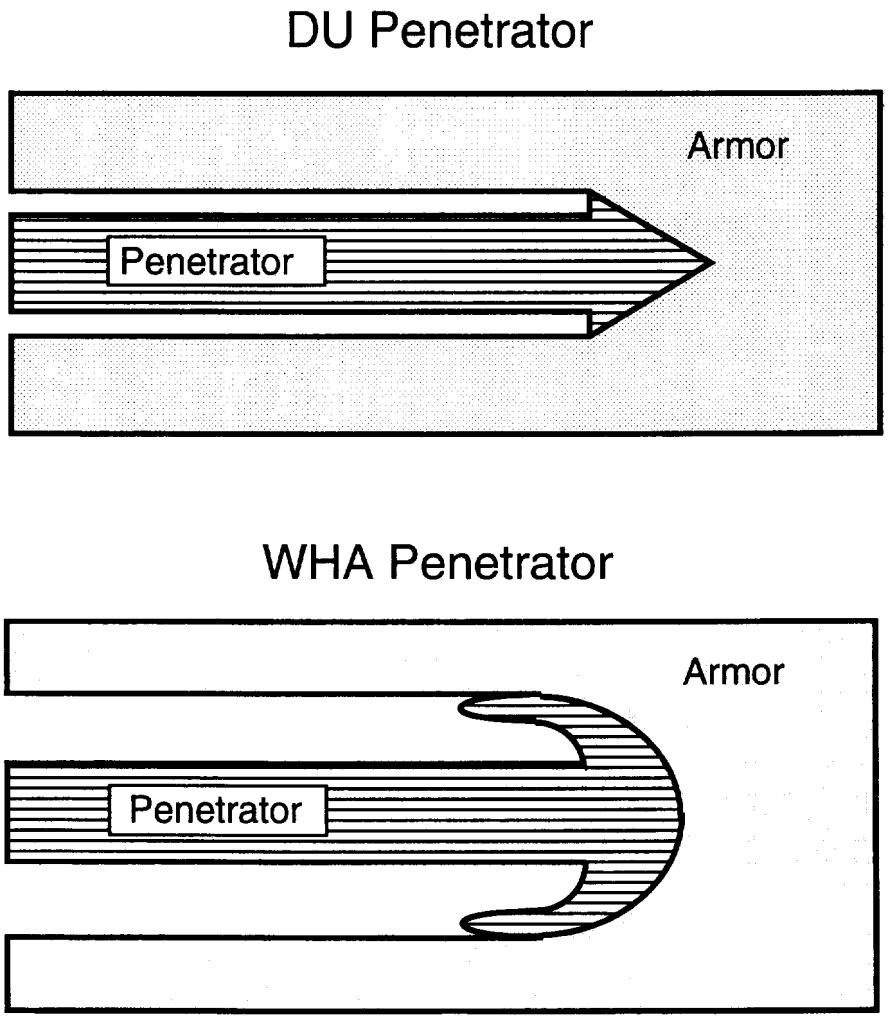


Fig. 1. Schematic of deformation of the depleted uranium (DU) and tungsten heavy alloy (WHA) penetrators during penetration.

the penetration tunnel and allow the projectile to penetrate more effectively. It appears that low strain rate sensitivity, low thermal conductivity, high heat capacity and a high rate of thermal softening contribute to the localized shear failure of DU alloys.

The lack of shear localization is believed to be responsible for the formation of a stable mushroom-head in tungsten heavy alloys (Magness, 1994). During dynamic deformations, the alloys demonstrate both strain hardening and strain rate hardening which, in combination with the large strains and high strain rates associated with penetration, result in a stabilizing mechanism with respect to shear localization (Rabin and German, 1988; Coates and Ramesh, 1991; Zurek *et al.* 1992). Specifically, at high strain rates, the flow stress of the alloy can be much higher than the quasi-static flow stress, thus the material becomes much harder to flow in a large shear deformation zone which would otherwise form a localized shear band. Further, a high hydrostatic pressure builds up during the penetration process, shutting down failure mechanisms such as microcracking and voiding that may also serve as initiators for localization. Consequently, a stable mushroom head is formed, and the penetrator material flows back only after large plastic strain has occurred, leading to a loss of penetration efficiency. In energy terms, this hypothesis is based on the premise that (assuming frictional terms remain of the same order of magnitude) a KE penetrator that undergoes localized deformations absorbs less of its kinetic energy in the plastic deformation of the penetrator material, since the plastic work is localized within a smaller volume. Thus more of the kinetic energy is available for processes that defeat the armor, leading to improved ballistic performance.

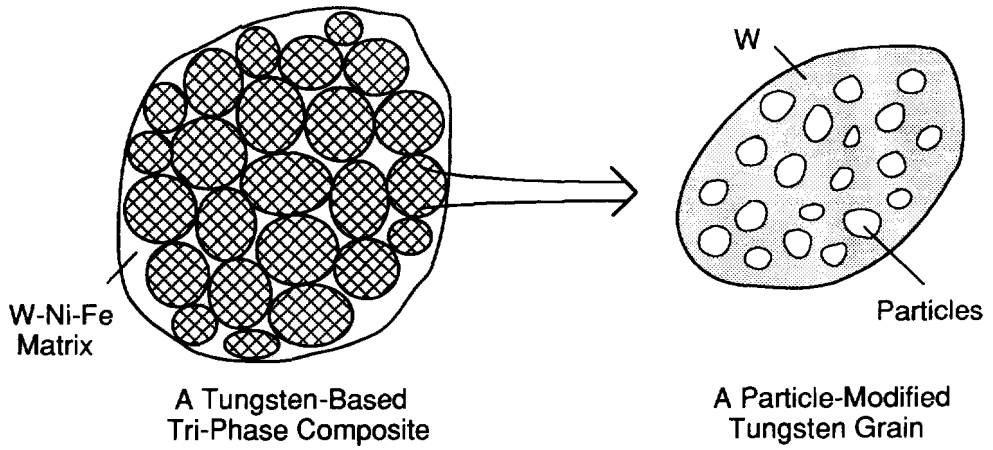


Fig. 2. Schematic of a tungsten-based composite composed of particle-modified tungsten grains embedded in a relatively soft matrix.

To significantly enhance the thermal softening and reduce the strain rate hardening of the tungsten heavy alloys, it is necessary to modify the pure tungsten phase, as it forms the dominant fraction of a WHA. As proposed recently by Ramesh (1995), a viable approach is to develop a tungsten-based composite (WBC) system comprised of particle modified tungsten grains embedded in a relatively soft matrix, as shown schematically in Fig. 2. The particle phase, be it metal or ceramic, thermally softens and melts at a relatively low temperature. Upon dynamic loading, both the tungsten phase and the matrix undergo large plastic deformation. Most of the work done ($\sim 90\%$) by such a deformation is converted to heat, elevating the temperature in the composite, causing thermal softening of the particles. Consequently, the overall composite flow stress decreases with strain at large strain rates, thus fostering the shear localization (Ramesh, 1995).

In order to realize the scenario just described for particle modified WBC, a number of issues must be addressed. The first issue concerns the selection of the proper particle material with desired thermal softening behavior. The second issue is the determination of optimal size and volume fraction of the particles. The third pertains to whether the particle modified WBC is indeed more susceptible to shear localization. The fourth issue is how to fabricate the particle modified WBC that has good chemical bonding at the particle/tungsten interface. Since the development of particle modified WBCs is still at its very early stage, the design of the microstructural features of the WBC is critically important.

To address the above-mentioned issues and to guide the design of the advanced WBCs for penetration applications, in this study, the rate-dependent stress-strain behavior of the particle modified tungsten-based composite is predicted systematically using a micromechanics approach. A survey is conducted first of the temperature-dependent elastic behavior of a wide range of materials, including ceramics, metals and intermetallics. The temperature-dependent elastic moduli of the particles are characterized by a set of exponential functions containing two non-dimensional parameters and a reference temperature. Identified as a candidate particle material, the behavior of soda-lime glass is used as a prototype in the modelling of the particles. Thermal softening of the composite under overall adiabatic compression are quantified using an axisymmetric finite element cell model with different temperature-dependent behaviors, sizes, volume fractions of the particle phase and different applied strain rates. Trends in the composite rate-dependent thermal softening behavior as determined by the controlling parameters are uncovered. The model developed and the results generated can provide guidance to the microstructural design of the particle modified tungsten-based composite in penetration applications.

## 2. THERMAL SOFTENING OF THE PARTICLE PHASE

The penetration application of the advanced WBC dictates the desired properties of the particle phase. Ideally, the particle material should have high density, low melting

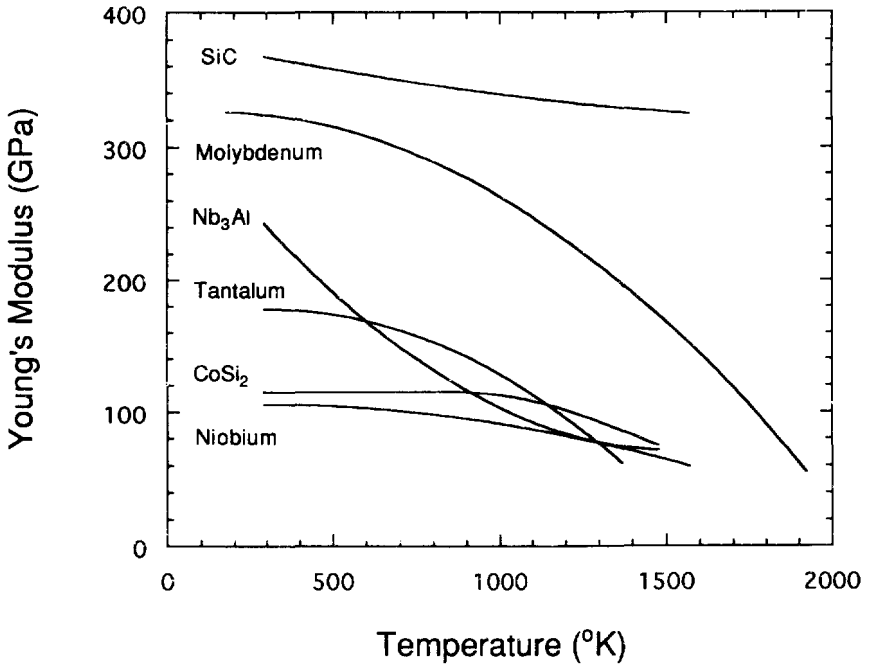


Fig. 3. Young's modulus vs temperature for various materials.

temperature, low thermal conductivity and diffusivity, and sufficiently high stiffness at room temperature. Thermal softening of the composite requires that the particle stiffness decays at relatively low temperature. To identify such a material, the temperature-dependent Young's moduli of several types of materials are investigated, including ceramics, heavy metals, and intermetallics. Some of the results are summarized in Fig. 3.

The temperature at which the particle phase should be sufficiently soft can be estimated as follows. Assume that 90% of the work done due to plastic deformation of tungsten is converted to heat. Under adiabatic compression, the temperature change $\Delta T$ in tungsten can be estimated using

$$\Delta T = \frac{0.9\sigma\varepsilon}{c_p\rho} \tag{1}$$

where $\sigma$ and $\varepsilon$ are true stress and strain, respectively, $\rho = 19250$ kg m$^{-3}$ is the density and $c_p = 132.5$ J kg$^{-1}$ K$^{-1}$ is specific heat of tungsten. If the tungsten phase experiences a 70% true strain during adiabatic compression with strain rate $\dot{\varepsilon} = 10^5$ 1/s, then the flow stress of tungsten is approximately $\sigma = 4$ GPa. We thus have $\Delta T = 988$ K. This implies that the particle phase should be sufficient soft or melt at about $T \approx 1000$ K.

Most of the materials surveyed are found to be not suitable as the particle material to modify tungsten (Syre, 1965; Parker, 1967; Rall *et al.*, 1976; Fukuhara and Abe, 1993; Anton and Shah, 1994; Shackelford, 1995). As can be seen from Fig. 3, silicon carbide (SiC) has Young's modulus that does not drop much as the temperature increases up to 1600 K. Some other carbide and oxide ceramics exhibit a similar trend. Metals similar to tungsten in the periodic table such as Molybdenum, Tantalum and Niobium have Young's moduli decreasing with temperature in a significant fashion but their melting temperatures are too high. Inter-metallics such as $Nb_3Al$ looks promising in that its Young's modulus drops rapidly with temperature. However, even at 1500 K, it is still too stiff to significantly reduce the flow behavior of tungsten at high strains.

As a candidate particle material, soda-lime glass exhibits a significant decay in Young's modulus $E$ when temperature $T$ is above 750 K; its melting temperature is at around

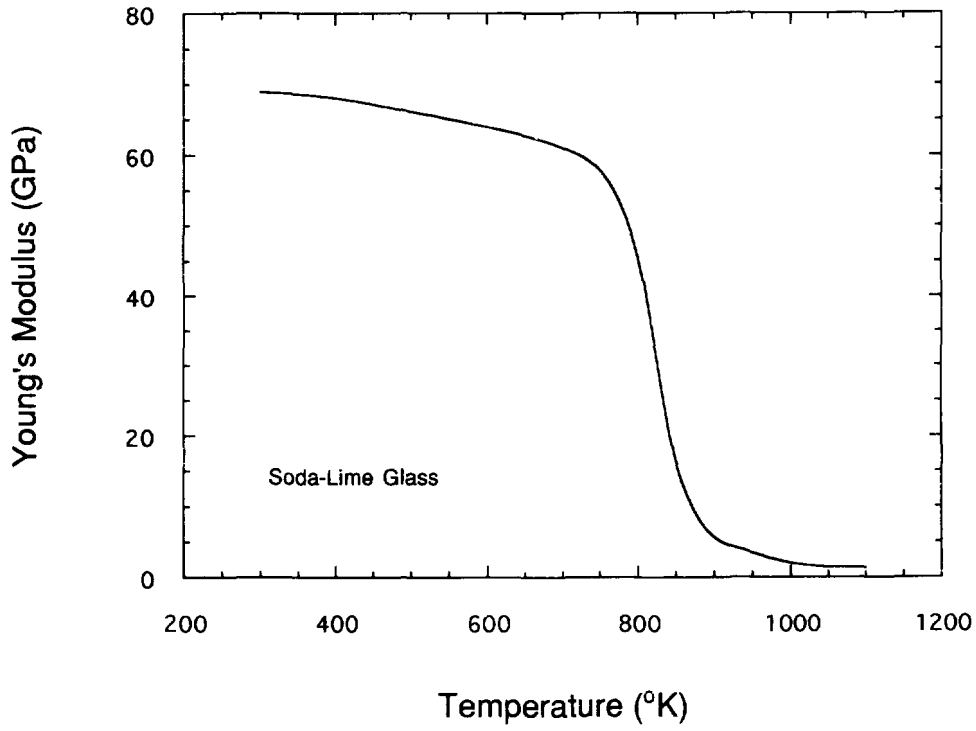


Fig. 4. Young's modulus vs temperature for soda-lime glass.

1000 °K (Syre, 1965), as shown in Fig. 4. When embedded in tungsten, this remarkable feature allows glass particles to thermally soften at relatively low strains and strain rates. Although only about 1/6 of that of tungsten, the stiffness $E_0$ of soda-lime glass at room temperature ( ~ 69 GPa) is acceptable. Further, the brittleness of glass at room temperature may not be a concern in modifying tungsten due to the high hydrostatic pressure in the WBC during penetration. The fabrication of a tungsten-based composite having uniformly distributed glass particles in the tungsten grains is feasible; the size and volume fraction of the particles can be controlled (Nagle, 1995). Attention in this paper is thus restricted to glassy particle materials such as soda-lime glass.

To mimic the thermal softening behavior of glass particles, a mathematical model is developed to characterize the temperature-dependent elastic properties of the glass phase. As a first-order approximation, the glass particles are taken to be homogeneous, isotropic linear elastic; viscosity and nonlinearity of the glass at high temperatures are neglected. Based on the behaviour of soda-lime glass shown in Fig. 4, the following exponential formulae are employed to represent respectively Young's modulus and Poisson's ratio of the particle phase as a function of temperature $T$ (in °K)

$$E(T) = E_0 \exp\left[-\beta\left(\frac{T-T_r}{T_0}\right)^{\alpha}\right] \tag{2}$$

$$\nu(T) = 0.5-(0.5-\nu_0)\exp\left[-\beta_\nu\left(\frac{T-T_r}{T_0}\right)^{\alpha_\nu}\right] \tag{3}$$

where $E_0$ and $\nu_0$ are, respectively, Young's modulus and Poisson's ratio of the particles at room temperature $T_r = 298$ °K, $T_0$ is a reference temperature, and $\alpha$, $\beta$, $\alpha_\nu$, $\beta_\nu$ are non-dimensional parameters. For any given glassy material, $\alpha$, $\beta$ and $T_0$ can be determined from the $E$ vs $T$ curve. For example, the behavior of soda-lime glass shown in Fig. 4 gives $\alpha = 7.47$, $\beta = 3.72$, $T_0 = 707$ °K. The determination of the parameters $\alpha_\nu$ and $\beta_\nu$ in (3) is difficult since not much data is available for $\nu$(T). In general, $\alpha_\nu \geqslant \alpha$, $\beta_\nu > \beta$ should be taken

to ensure that the particle phase becomes incompressible as it melts. This implies that Poisson's ratio $\nu$ approaches 0.5 faster than the stiffness $E$ approaches zero. Since thermal softening of the particles is largely controlled by its stiffness $E$, in this study, we assume that $\alpha_\nu = \alpha$, $\beta_\nu = \beta$. Consequently, the bulk modulus remains finite as temperature $T$ becomes large. However, the effect of the resulting compressibility of the particles is very small, as will become clear later. To further limit the number of variables, in all the calculations performed, $T_0$ in (2) and (3) was taken to be 707 °K.

The expressions for the temperature-dependent Young's modulus $E(T)$ and Poisson's ratio $\nu(T)$ given in (2) and (3) respectively can be used to simulate a wide range of particle materials especially glass. Shown in Fig. 5a is the normalized Young's modulus $E(T)/E_0$ as a function of the nondimensional temperature $(T-T_r)/T_0$ for $\beta = 3.72$, $\alpha = 2$, 4, 6, 7.42 and 10. Clearly, at room temperature, $E = E_0$; at melting temperature, $E \approx 0$. The transition between these two limits depends on the value of $\alpha$: a low $\alpha$ leads to an early onset of softening and a smooth transition, while a high $\alpha$ gives the opposite. The influence of $\beta$ on $E(T)$ is shown in Fig. 5b where curves of $E(T)/E_0$ vs $(T-T_r)/T_0$ are displayed for $\alpha = 7.42$, $\beta = 1$, 2, 3.72 and 6. Evidently, when $\beta$ is large (e.g., $\beta = 6$), the rapid decay in $E$ occurs at a lower temperature. Roughly speaking, when $\beta$ decreases, the $E$ vs $T$ curve shifts to the right, but the onset of softening remains almost unchanged. Similar trends are true for Poisson's ratio $\nu(T)$, as can be seen from the functional forms of $E(T)$ and $\nu(T)$ given in eqns (2) and (3).

## 3. THE MICROMECHANICAL CELL MODEL

With glassy particles embedded in the tungsten grains, the stress-strain behavior of a tungsten based composite is expected to exhibit thermal softening at large strains. To quantify the effect of thermal softening of the particles on the composite behavior, a micromechanical cell model is developed to solve the coupled stress-heat transfer problem. To gain insight, only pure tungsten grains containing glassy particles are considered in the modeling. For convenience, in the rest of this paper, we denote the tungsten phase by "matrix". It is assumed that the particles are spherical, equal-sized, and uniformly distributed in the matrix. Consequently, the dual-phase, tungsten matrix/glass particle composite can be represented by a unit cell composed of a single spherical particle embedded in the matrix, as depicted in Fig. 6. The hexagonal cell is further approximated by a cylindrical cell in order to form an axisymmetric cell model, which is computationally advantageous (Bao *et al.*, 1991; Bao and Ramesh, 1993; Bao and Lin, 1996). The aspect ratio of the cell is taken to be unity. The volume fraction of the particles $f$ is taken to be the ratio of the particle volume to the cell volume. The axisymmetric cell in Fig. 6 is constrained such that the cylindrical surface remains cylindrical and the ends remain planar. Under overall uniaxial compression, the average normal stress on the ends is $\bar{\sigma}$, and the average normal tractions on the cylindrical surface and the shear tractions on the cylindrical sides and the ends are zero.

Following Bao and Ramesh (1993), the quasi-static uniaxial stress-strain behavior of the tungsten matrix is characterized by a Ramberg-Osgood type power-law relationship between the quasi-static flow stress $\sigma_s$ and the axial strain $\varepsilon$

$$\frac{\varepsilon}{\varepsilon_0} = \frac{\sigma_s}{\sigma_0} + \alpha_0 \left(\frac{\sigma_s}{\sigma_0}\right)^n \tag{4}$$

where $\sigma_0 = 1$ GPa is a reference stress, $n = 11.75$ is the stress exponent, $\alpha_0 = 0.132$, $\varepsilon_0 = \sigma_0/E_m$, with $E_m = 400$ GPa being Young's modulus of pure tungsten. The strain-rate hardening of the tungsten matrix is assumed to obey an over-stress model (Bao and Lin, 1996).

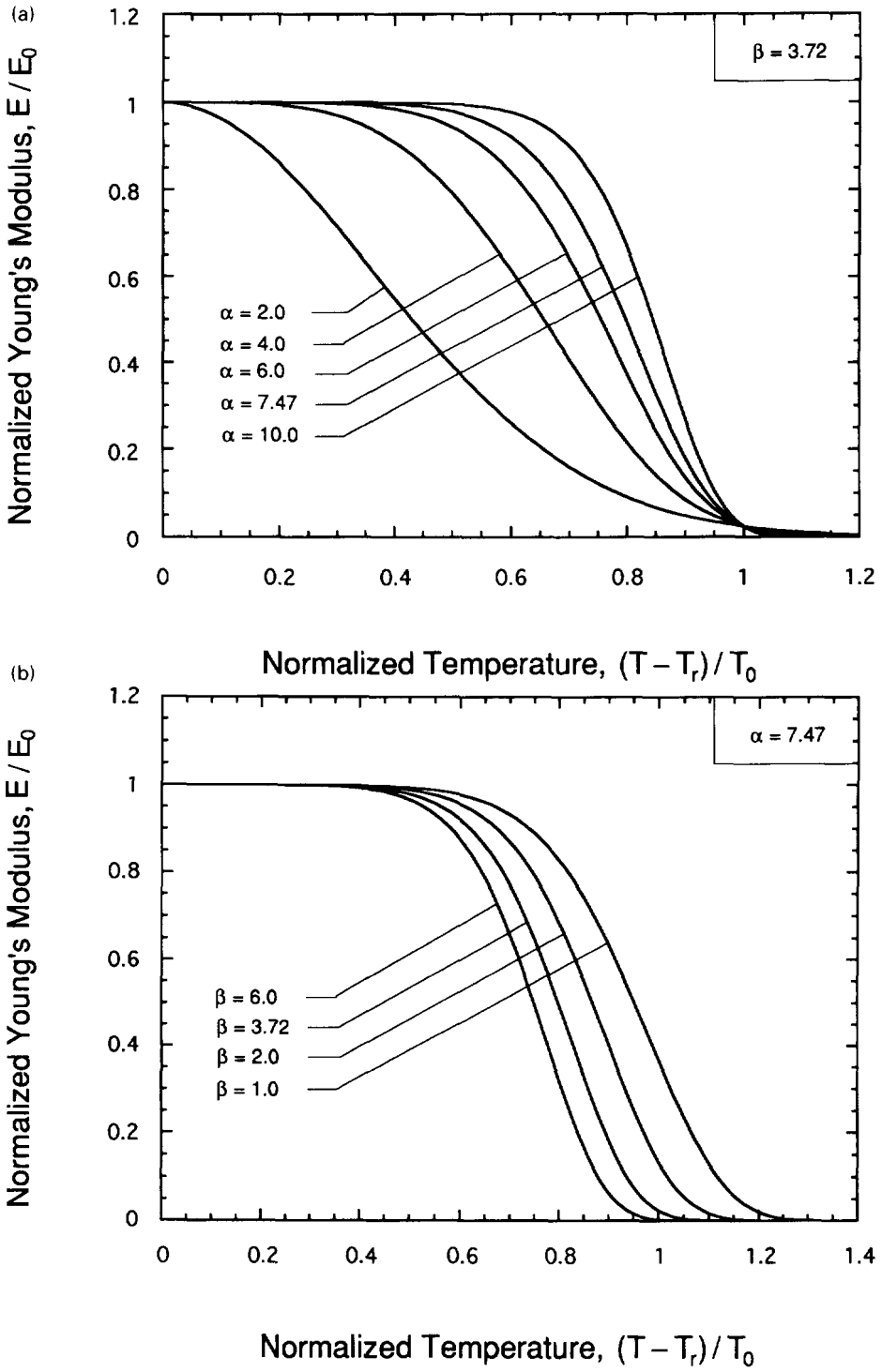


Fig. 5. Normalized Young's modulus vs nondimensional temperature as determined by the mathematical model in eqn (2) (a) for different values of $\alpha$ and (b) for different values of $\beta$.

$$\dot{\varepsilon}^p = \dot{\varepsilon}_0 \left( \frac{\sigma}{\sigma_s} - 1 \right)^{1/m} \tag{5}$$

where $\dot{\varepsilon}^p$ is the plastic strain rate, $\dot{\varepsilon}_0 = 10^5\ \mathrm{s}^{-1}$ is a reference strain rate, and $m = 0.18$ is the strain-rate hardening exponent (Zhou *et al.*, 1994). Under high strain rate deformation, the tungsten phase can exhibit substantial thermal softening (Zhou *et al.*, 1994). However, to

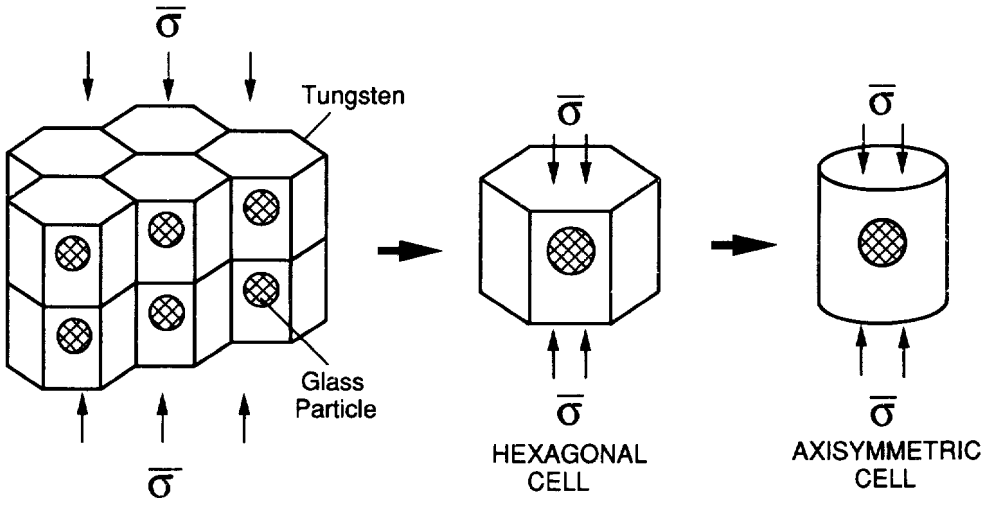


Fig. 6. The unit cell model for a particle-modified tungsten matrix composite.

show more clearly the effect of thermal softening of the particles on the behavior of the composite, in this study, the effect of thermal softening of tungsten is excluded.

Equations (4) and (5) can be combined to give a rate dependent Ramberg-Osgood type stress-strain relation

$$\frac{\varepsilon}{\varepsilon_0} = \frac{\sigma}{\hat{\sigma}_0} + \alpha\left(\frac{\sigma}{\hat{\sigma}_0}\right)^n \tag{6a}$$

where $\hat{\sigma}_0$ is a new reference stress

$$\hat{\sigma}_0 = \sigma_0\left[1 + \left(\frac{\dot{\varepsilon}^p}{\dot{\varepsilon}_0}\right)^m\right]. \tag{6b}$$

Note that the form of the stress-strain relation in (6a) is identical to that of a rate-independent Ramberg-Osgood material. Emphasis in this study is placed on the composite behavior at large strains; the effect of elastic strain rate on the composite behavior is negligible. Thus, for a homogeneous matrix material, $\dot{\varepsilon}^p \approx \dot{\varepsilon}$ where $\dot{\varepsilon}$ is the overall applied strain rate, and

$$\sigma_0^r = \sigma_0\left[1 + \left(\frac{\dot{\varepsilon}}{\dot{\varepsilon}_0}\right)^m\right]. \tag{6c}$$

can be used as the rate-dependent reference stress for the matrix material.

As described in more detail in the previous section, the particle material is taken to be isotropic, linear elastic, with the temperature-dependent Young's modulus $E(T)$ and Poisson's ratio $\nu(T)$ given in (2) and (3), respectively. Since the possible debonding cracking at the particle/matrix interface is likely to be suppressed by the high hydrostatic pressure in the material during penetration, it is assumed that the interface is perfectly bonded.

To realize thermal softening of the particles during deformation, heat transfer from the matrix to the particles must be considered in the analysis. For simplicity, the unit cell shown in Fig. 6 is assumed to be in an adiabatic state under uniaxial compression, although heat conduction and temperature redistribution prevail both within and between the tungsten grains during penetration. Consequently, only heat transfer between the particle and tungsten matrix is allowed; the cylindrical surface and the two ends of the axisymmetric unit cell are taken to be thermally insulated. This adiabatic assumption is reasonable since

Table 1. Thermophysical properties of tungsten and soda-lime glass

| Material | Density kg m$^{-3}$ | Specific heat J kg$^{-1}$ K$^{-1}$ | Thermal conduct. W m$^{-1}$ K$^{-1}$ |
|---|---|---|---|
| Tungsten | 19250 | 132.5 | 178.0 |
| Soda-lime glass | 2470 | 754.0 | 83.74 |

the time scale associated with the high rate of deformation only allows heat transfer to occur locally, for example, from the matrix to the particles.

The heat transfer problem requires the specification of density $\rho$, specific heat $c_p$ and thermal conductivity $\lambda$ for each phase; the values of these material constants are compiled in Table 1. In all the calculations performed, the inelastic heat fraction—the fraction of the plastic work that converted to heat—is taken to be 0.9.

The heat transfer problem defines an intrinsic length scale $L_0$. To illustrate, consider the equation of heat transfer

$$\frac{\partial T}{\partial t} - \kappa \nabla^2 T = 0 \tag{7}$$

where $T(x, y, z, t)$ is the temperature distribution at time $t$, $\nabla^2$ is the Laplace operator, and $\kappa = \lambda/\rho c_p$ is the thermal diffusivity. The nondimensional form of eqn (7) introduces a dimensionless parameter $\eta$

$$\eta = \frac{\lambda t_0}{\rho c_p L_0^2} \tag{8}$$

which gives a thermal diffusion length scale $L_0$

$$L_0 = \sqrt{\frac{\lambda t_0}{\rho c_p}} \tag{9}$$

where $\eta$ is taken to be unity. Note that in eqn (9), $t_0$ is a time scale specific to the physical process under study. Due to the existence of the intrinsic length scale $L_0$, the particle size in the finite element cell model described above for the coupled stress-heat transfer problem cannot be defined arbitrarily.

A finite element method was used to calculate the overall uniaxial stress-strain behavior of the composite under adiabatic compression. The commercial finite element code ABAQUS was employed to solve the nonlinear, coupled stress-heat transfer boundary value problems for the axisymmetric cell, using 8-noded biquadratic elements. Due to symmetry, only half of the unit cell needs to be discretized. A typical finite element mesh is shown in Fig. 7. In calculating the stress-strain curve of the composite, the upper surface of the unit cell is constrained to have the same displacement in the $z$-direction. A displacement $u_z$ of the upper surface is then applied according to the desired overall strain and strain rate. The overall stress of the composite is obtained by dividing the reaction force $F$ at the upper surface with the surface area $A$. The stress-strain curves were computed incrementally with a fixed overall strain rate $\dot{\bar{\varepsilon}}/\dot{\varepsilon}_0$ and a fixed strain increment $\Delta\bar{\varepsilon}/\varepsilon_0$. Typically, at least 200 increments were taken to calculate each curve for true strains $\bar{\varepsilon}$ up to 190% (applied nominal strain up to 85%). For convenience, in the finite element analysis, the units used for length, force, time and temperature are respectively micron ($10^{-6}$ m), millinewton ($10^{-3}$ N), microsecond ($10^{-6}$ s), and degree Kelvin (°K).

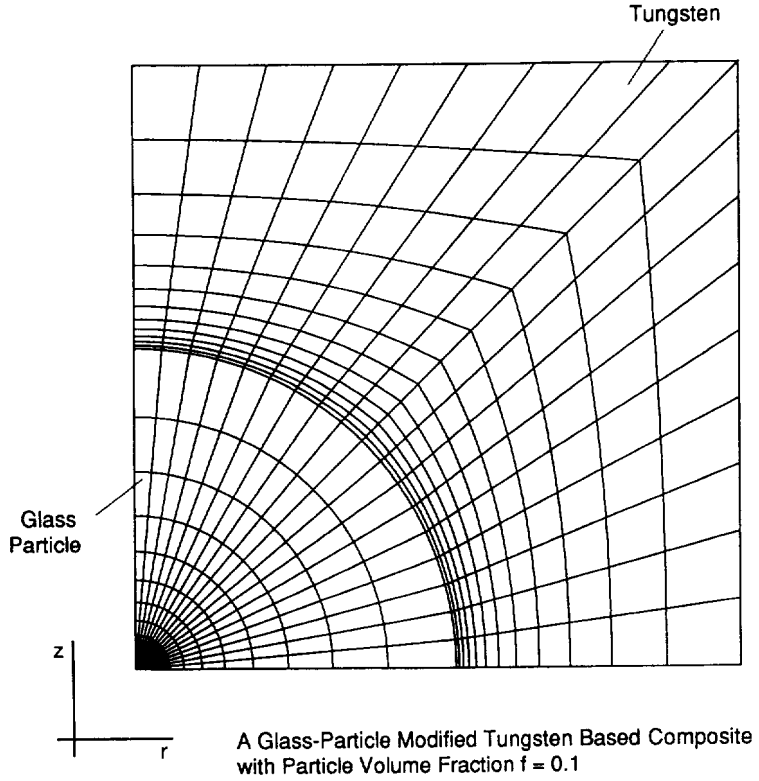


Fig. 7. A typical finite element mesh for the axisymmetric unit cell representing a particle-modified tungsten matrix composite.

## 4. THERMAL SOFTENING OF COMPOSITE

To aid the microstructural design of particle-modified tungsten-based composites, predictions are made for the overall stress-strain behavior of the composite under adiabatic compression. Shown in Fig. 8 is the overall flow stress as a function of true strain under applied strain rate $\dot{\varepsilon}/\dot{\varepsilon}_0 = 1.0$ for pure tungsten, and tungsten matrix composites containing respectively non-softening particles, glassy particles and incompressible pores. The volume fraction and radius of the particles are taken to be $f = 0.1$ and $r = 0.5$ $\mu$m, respectively. The parameters characterizing thermal softening of the particles are taken as $\alpha = 7.47$, $\beta = 3.72$. As demonstrated in Fig. 8, the deformation of the composite has three stages. (1) When the overall strains $\bar{\varepsilon}$ are small, the temperature increase $\Delta T$ in the tungsten phase is not high enough to cause particle softening; the glass particles behave elastically. The composite stress-strain behavior is identical to that of a tungsten matrix composite reinforced with elastic particles. (2) When $\bar{\varepsilon}$ is large, the heat generated in tungsten is transferred to the glass particles, causing them to soften; the composite overall flow stress decreases with strain until the particles are completely melted. (3) With further increase of the overall strain, the stress-strain behavior is identical to that of a tungsten matrix composite containing incompressible pores (Bao, 1996). Obviously, due to plastic deformation, temperature in the glass particle modified tungsten matrix composite increases with the overall strain $\bar{\varepsilon}$, as illustrated by Fig. 9.

The stress-strain behavior of glass-particle modified tungsten composite (WBC) shown in Fig. 8 has important implications. Compared with pure tungsten, the WBC can have a much lower flow stress at large strains and strain rates, thus fostering the shear localization. Further, the higher flow stress at low strains may reduce the overall deformation of the penetrator head, giving rise to a smaller head and leaving more kinetic energy to defeat the armor. Finally, the molten glass particles may also serve as the initiation sites for localized shear bands.

When the particles are fully melted, they can be taken as incompressible fluid with no resistance to shear deformation. As uncovered recently by Bao (1996) in studying the rate

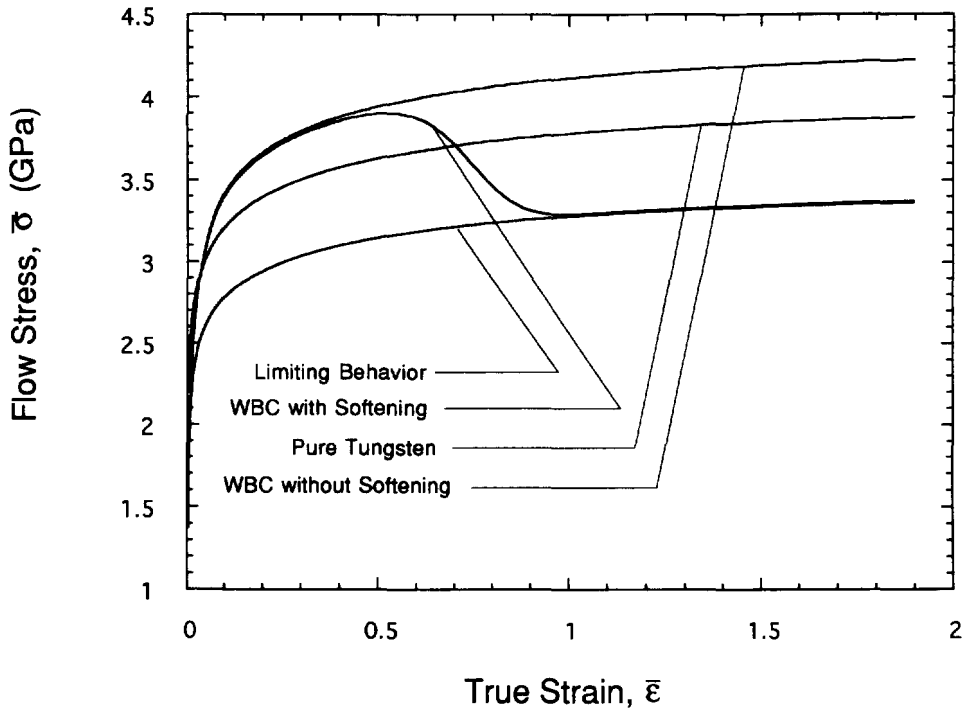


Fig. 8. Comparison of the overall flow stress as a function of true strain for pure tungsten, a particle reinforced tungsten matrix composite without thermal softening, a glass particle modified tungsten matrix composite with thermal softening, and a tungsten matrix composite containing incompressible pores.

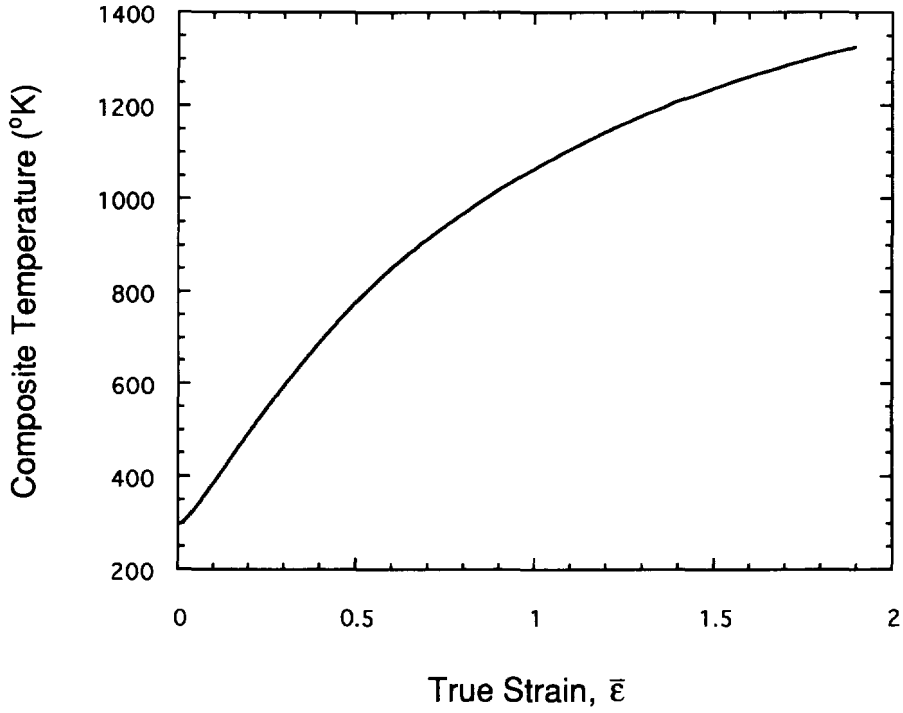


Fig. 9. Temperature in the glass particle modified tungsten matrix composite as a function of true strain. The temperature increase is due to plastic deformation in tungsten; 90% of the plastic work is converted to heat.

dependent behavior of metal matrix composites containing incompressible spherical pores, within a few percent error, the stress $\bar{\sigma}$ vs strain $\bar{\varepsilon}$ curve of the composite under uniaxial tension or compression can be described by

$$\frac{\bar{\varepsilon}}{\varepsilon_0} = \frac{\bar{\sigma}}{\sigma_0^r}\frac{\bar{E}}{E_m} + \alpha_0\left(\frac{\bar{\sigma}}{\sigma_0^r}\frac{1}{\phi}\right)^n \tag{10}$$

where

$$\phi = \exp(-1.5634f) \tag{11}$$

represents the reduction in composite flow stress due to the pores,

$$\frac{\bar{E}}{E_m} = 1 + \frac{f\left(\frac{E_0}{E_m} - 1\right)}{1 + (1-f)\left(\frac{E_0}{E_m} - 1\right)\left(3\frac{1-\nu_0}{1+\nu_0}\right)^{-1}} \tag{12}$$

is the composite Young's modulus $\bar{E}$ normalized by that of the matrix $E_m$ (Christensen, 1991), $f$ is the volume fraction of the particles (pores). Poisson's ratio of the matrix is taken to be that of the particles at room-temperature, $\nu_0$. The parameters $\alpha_0$, $\varepsilon_0$ and $n$ in (10) are the same as those of the matrix material given in (6a); the reference stress $\sigma_0^r$ is that defined in (6c). As demonstrated by the curves in Fig. 8, the stress-strain behavior given by the analytical formula in (10) is almost identical to the finite element results at large strains. This implies that the effect of the compressibility of the particles at high temperatures as a result of taking $\alpha_v = \alpha$, $\beta_v = \beta$ in (3) is negligible, since the formula given in (10) is based on the behavior of a composite containing incompressible pores. In the rest of this paper, the composite behavior characterized by (10) is referred to as the "limiting behavior".

The thermal softening behavior of the tungsten-based composite depends on the applied strain rate $\dot{\varepsilon}$, and the softening behavior (in terms of $\alpha$ and $\beta$), volume fraction $f$ and radius $r$ of the glass particles. To uncover the relative roles of each of these five parameters, their values are varied systematically in the finite element calculations. Displayed in Fig. 10 are curves of the normalized composite flow stress $\bar{\sigma}/\sigma_0^r$ vs true strain for $f = 0.1$, $r = 0.5$ $\mu$m, $\alpha = 7.47$, $\beta = 3.72$ for applied strain rates $\dot{\varepsilon}/\dot{\varepsilon}_0 = 0.001$, 0.01, 0.1, 1.0 and 5.0. It is seen that thermal softening occurs early and develops fast when the strain rate is high; the opposite is true when the strain rate is low. The applied strain $\bar{\varepsilon}_c$ at which the particles become completely "melted" (i.e., become incompressible pores) increases with decreasing strain rate. Note that for strains $\bar{\varepsilon} > \bar{\varepsilon}_c$, all the $\bar{\sigma}/\sigma_0^r$ versus true strain curves with different strain rates follow the same limiting curve.

As mentioned earlier, the heat-transfer problem defines an intrinsic length scale $L_0$ given in (9). Thus, in general, the composite thermal softening behavior changes with particle size. If the time scale for the formation of localized shear band during penetration is taken to be 10 $\mu$s, then for pure tungsten $L_0 = 26.4$ $\mu$m. It is therefore reasonable to believe that for particle sizes much less than $L_0$, the size effect is negligible. Figure 11 shows the stress-strain curves of a composite with $f = 0.1$, $\alpha = 7.47$, $\beta = 3.72$, $\dot{\varepsilon}/\dot{\varepsilon}_0 = 1.0$ with particle radius $r = 0.2$, 0.5, 1.0, 2.0, 5.0, 10.0 and 20.0 $\mu$m. Indeed the effect of particle size is negligible for $r \leqslant 5$ $\mu$m; the stress-strain curves are almost identical for $0.2$ $\mu$m $\leqslant r \leqslant$ 2.0 $\mu$m. For a composite with different particle volume fractions and subjected to different applied strain rates, it is anticipated that the size effect remains roughly the same as that shown in Fig. 11. For composites with particle radius $r \geqslant 10.0$ $\mu$m, attempts have been made unsuccessfully to calculate the complete stress-strain curves due to severe numerical problems. Since in most tungsten heavy alloys the grain size is less than 100 $\mu$m, the radius of the glass particles is expected to be less than 10 $\mu$m. Thus, the range of the particle radius covered in Fig. 11 is sufficiently large.

The effect of different particle thermal softening behaviors on the overall rate-dependent behavior of the composite is examined by changing the non-dimensional parameters $\alpha$ and $\beta$ in eqns (2) and (3). Displayed in Fig. 12a are stress-strain curves of the composite with $f = 0.1$, $r = 0.5$ $\mu$m, $\dot{\varepsilon}/\dot{\varepsilon}_0 = 1.0$, $\beta = 3.72$ with $\alpha = 2$, 4, 6, 7.47 and 10 (note that for

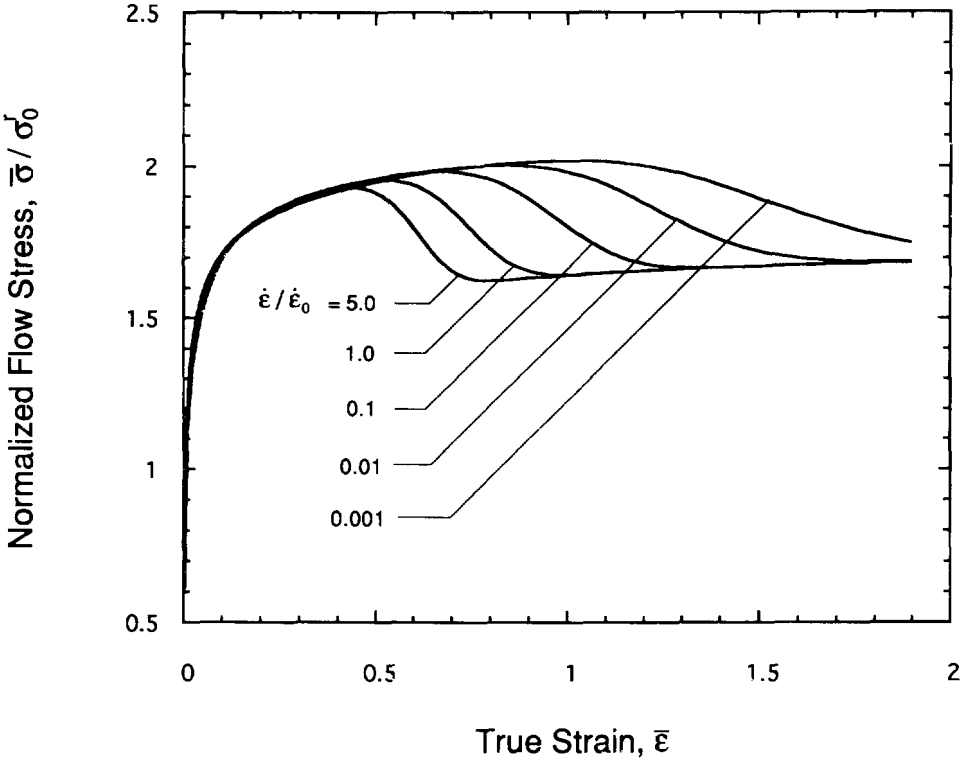


Fig. 10. Normalized composite flow stress vs true strain for a glass particle modified tungsten composite with $f = 0.1$, $r = 0.5\ \mu m$, $\alpha = 7.47$, $\beta = 3.72$ with different applied strain rates $\dot{\varepsilon}/\dot{\varepsilon}_0 = 0.001$, 0.01, 0.1, 1.0 and 5.0.

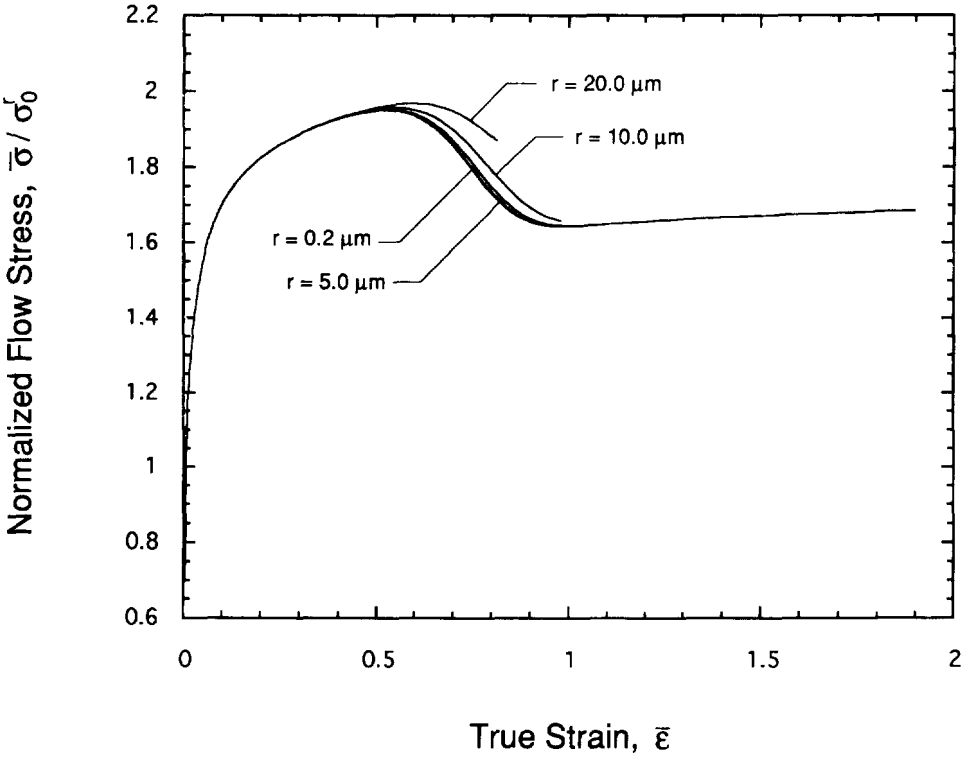


Fig. 11. Normalized composite flow stress vs true strain for a glass particle modified tungsten composite with $f = 0.1$, $\dot{\varepsilon}/\dot{\varepsilon}_0 = 1.0$, $\alpha = 7.47$, $\beta = 3.72$ with different particle radii $r = 0.2$, 0.5, 2.0 and 5.0 $\mu m$.

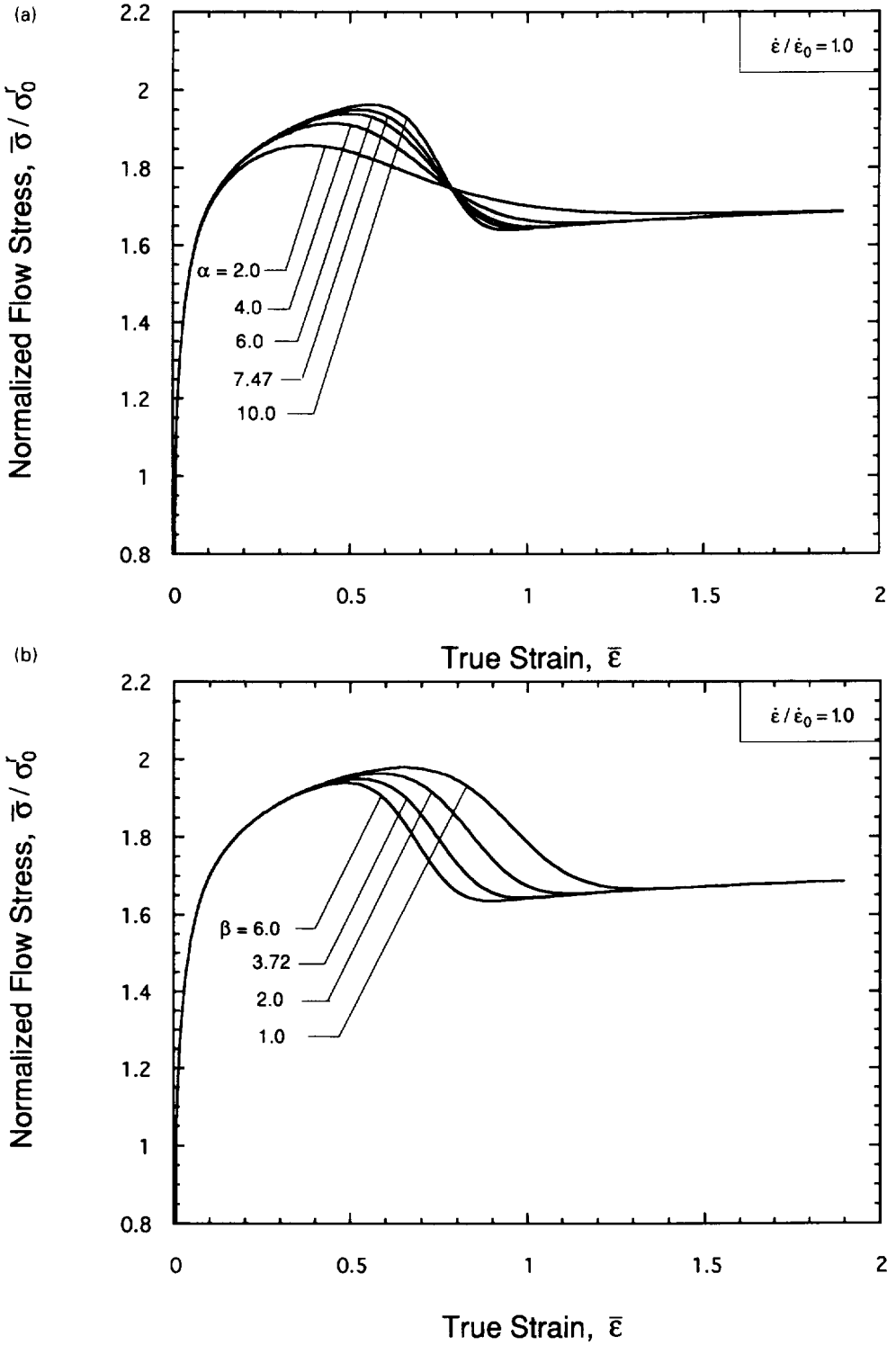


Fig. 12. Normalized composite flow stress vs true strain for a glass particle modified tungsten composite with $f = 0.1$, $r = 0.5$ $\mu$m, $\dot{\varepsilon}/\dot{\varepsilon}_0 = 1.0$ with (a) $\alpha = 2.0, 4.0, 6.0, 7.47, 10.0$ and with (b) $\beta = 1.0, 2.0, 3.72, 6.0$.

soda-lime glass, $\alpha = 7.47$, $\beta = 3.72$). Evidently, the value of $\alpha$ influences both the onset and the rate of thermal softening: a low of $\alpha$ (e.g., $\alpha = 2$) gives rise to a more gradual and an early onset of thermal softening, while with a large $\alpha$ thermal softening of the composite occurs late and more abruptly. The maximum composite flow stress is seen to increase with $\alpha$. The effect of changing $\beta$ is shown in Fig. 12b in which the normalized composite flow

stress $\bar{\sigma}/\sigma_0^r$ is plotted as a function of the true strain $\bar{\varepsilon}$ for $f = 0.1$, $r = 0.5$ $\mu$m, $\dot{\varepsilon}/\dot{\varepsilon}_0 = 1.0$, $\alpha = 7.47$ for $\beta = 1.0$, 2.0, 3.72 and 6.0. The onset of thermal softening of the composite is essentially independent of $\beta$; however, when $\beta$ is smaller, the thermal softening process spans over a larger range of strains, as demonstrated by Fig. 12b.

For a glass particle modified tungsten-based composite, the particle volume fraction $f$ is an important controlling parameter for the following reasons. First, $f$ can be well controlled in fabricating the composite. Second, the rate-dependent stress-strain behavior changes with $f$. Finally, the density of the composite decreases with increasing $f$, which is an important issue for a kinetic energy penetrator. To guide the composite microstructural design, stress-strain curves of the composite are calculated for particle volume fractions $0.05 \leqslant f \leqslant 0.25$ for different applied strain rates. Displayed in Fig. 13a are the $\bar{\sigma}/\sigma_0^r$ vs $\bar{\varepsilon}$ curves of the composite for $r = 0.5$ $\mu$m, $\alpha = 7.47$, for $\beta = 3.72$, $\dot{\varepsilon}/\dot{\varepsilon}_0 = 0.01$ for $f = 0.0$, 0.05, 0.1, 0.15, 0.2, 0.25. It is clear that, compared with the stress-strain behavior of pure tungsten, a high particle volume fraction (e.g., $f = 0.25$) can give rise to a much higher composite flow stress before softening, and a much lower flow stress after the particles are melted. Note that the limiting behavior of the composite is also dependent on the particle volume fraction. For penetration applications, the optimal particle volume fraction is dictated by two competing trends: a high particle volume fraction can lead to the desired stress-strain behavior of the composite but at the same time significantly reduce the density of the composite (and therefore the kinetic energy of the penetrator). The stress-strain curves of the composite with the same set of material parameters but with a different applied strain rate $\dot{\varepsilon}/\dot{\varepsilon}_0 = 1.0$ are shown in Fig. 13b. The general trends are similar to that shown in Fig. 13a. However, with a larger strain rate, the transition of the composite flow behavior from strengthening to softening occurs earlier and more abruptly.

Displayed in Fig. 14a is the composite flow stress as a function of the overall strain rate for a composite containing glass particles with $r = 0.5$ $\mu$m, $\alpha = 7.47$, $\beta = 3.72$, $f = 0.05$, 0.1, 0.15, 0.2 and 0.25. The flow stresses of the composite are taken at the true strain $\bar{\varepsilon} = 1.05$. Clearly, thermal softening of the glass particles reduces the strain-rate sensitivity of the tungsten-based composite. The reduction in strain-rate sensitivity depends on the particle volume fraction, as might be expected. When the overall strains are large (e.g., $\bar{\varepsilon} = 1.6$), the composite strain-rate sensitivity does not change much relative to that of tungsten for $0.01 \leqslant \dot{\varepsilon}/\dot{\varepsilon}_0 \leqslant 5.0$, as can be seen from Fig. 14b. Specifically, for $0.05 \leqslant f \leqslant 0.25$, the increase in composite flow stress $\Delta\sigma$ corresponding to an increase in strain rate $\Delta\dot{\varepsilon}$ is roughly the same as that of the tungsten matrix. This is due to the fact that at such a large strain the particles are fully melted over this range of strain rates.

## 5. CONCLUDING REMARKS

To improve the ballistic performance of the tungsten heavy alloy penetrators, an advanced tungsten-based composite (WBC) system composed of particle-modified tungsten grains embedded in a softer matrix is being developed. This new WBC material has the potential to possess better thermophysical properties such as a lower strain rate sensitivity and an enhanced susceptibility to shear localization. To help in realizing this potential, a micromechanics study is made of the thermal softening behavior of the composite. Specifically, the stress-strain curves of the composite under overall adiabatic compression are predicted using an axisymmetric finite element cell model with different temperature-dependent behaviors, sizes, volume fractions of the particle under different applied strain rates. Trends in the composite rate-dependent thermal softening behavior as determined by the controlling parameters are uncovered.

In designing the composition and microstructure of a particle-modified tungsten-based composite for penetration applications, it is necessary to chose the proper particle material that gives the desired thermomechanical behavior of the composite. Based on a survey of the temperature-dependent elastic behavior of a wide range of materials, the soda-lime glass is identified as a candidate particle material. A mathematical model is developed to describe the temperature dependence of Young's modulus and Poisson's ratio of the particle phase in terms of two nondimensional parameters $\alpha$ and $\beta$ and a reference temperature $T_0$.

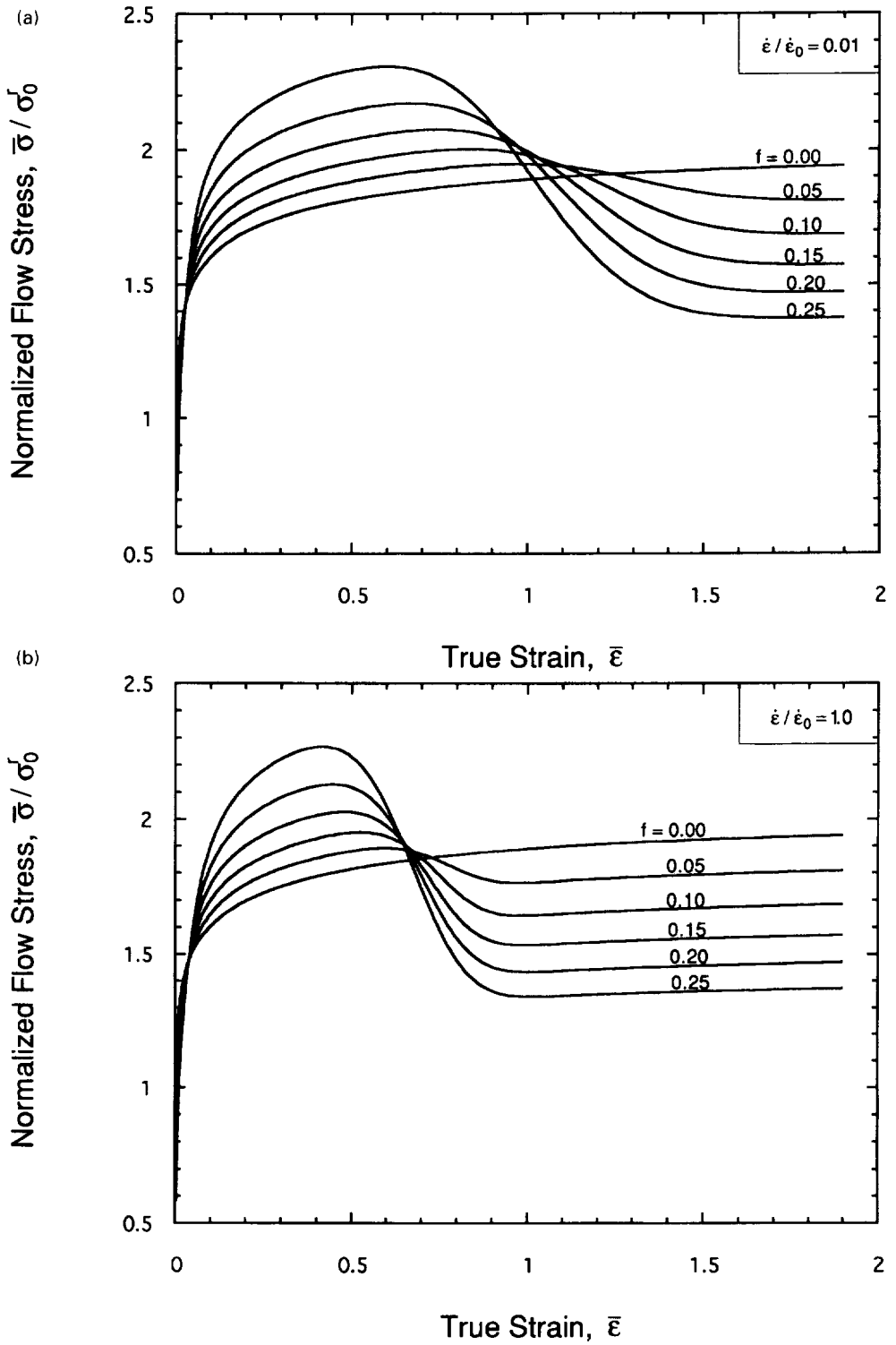


Fig. 13. Normalized composite flow stress vs true strain for a glass particle modified tungsten composite with $r = 0.5\ \mu m$, $\alpha = 7.47$, $\beta = 3.72$ with different particle volume fractions $f = 0.0, 0.05, 0.1, 0.15, 0.2$ and 0.25 under applied strain rate (a) $\dot{\varepsilon}/\dot{\varepsilon}_0 = 0.01$ and (b) $\dot{\varepsilon}/\dot{\varepsilon}_0 = 1.0$.

It is possible that materials other than glass can be used as the particle material; the model developed in this paper can be used for those materials as well.

For a given particle material, the composite rate-dependent thermal softening behavior depends on particle size, shape, volume fraction and distribution. To gain insight, in this study, it is assumed that particles are spherical and uniformly distributed although in reality

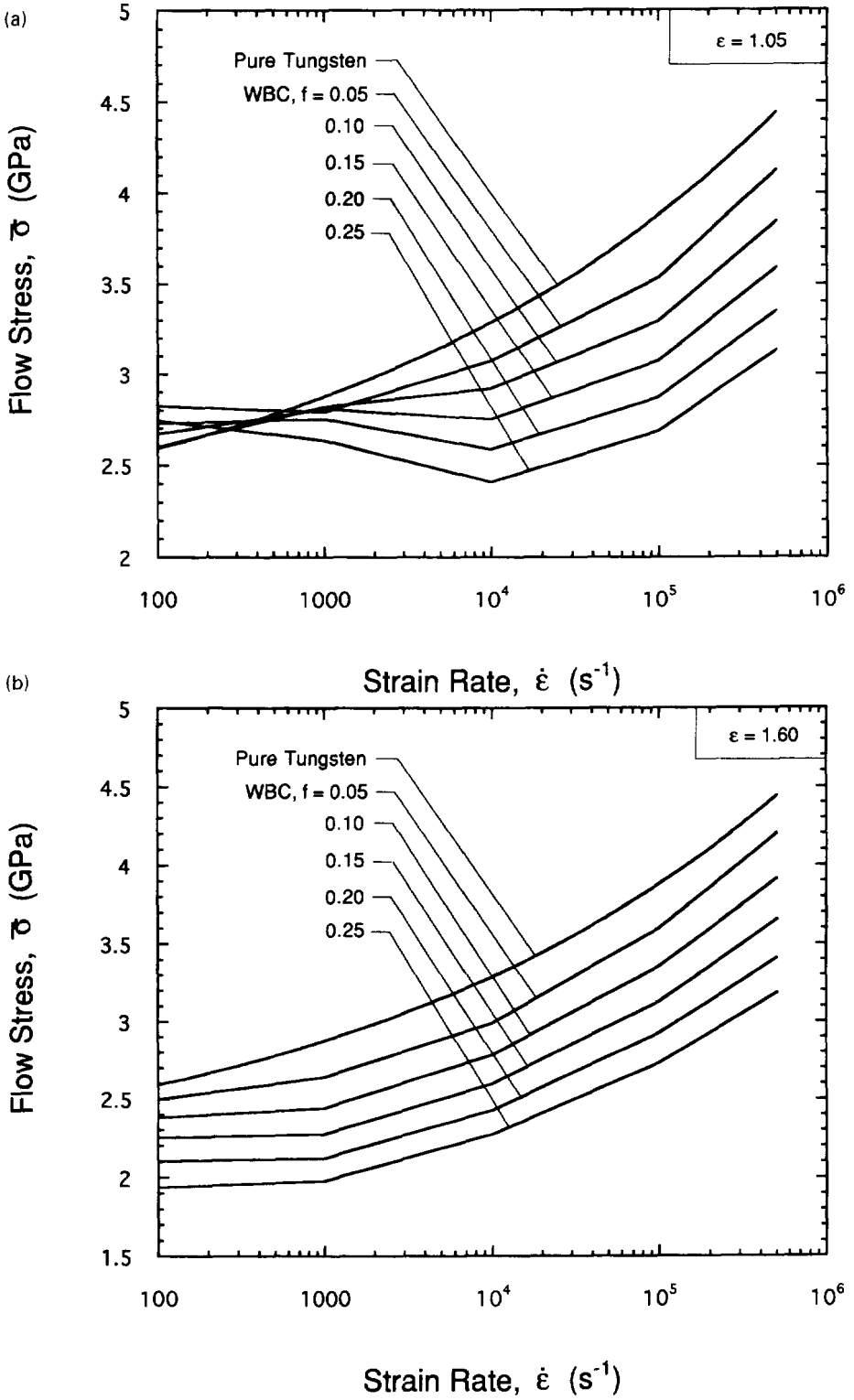


Fig. 14. Composite flow stress as a function of the applied strain rate for a glass particle modified tungsten composite with $r = 0.5$ μm, $\alpha = 7.47$, $\beta = 3.72$ with different particle volume fractions $f = 0.0, 0.05, 0.1, 0.15, 0.2$ and 0.25 at true strain (a) $\bar{\varepsilon} = 1.05$ and (b) $\bar{\varepsilon} = 1.6$.

the particle shape can be very irregular. It is further assumed that the particles are isotropic linear elastic; viscosity of the particles at high temperatures is neglected. It is anticipated that the viscous behavior of the particles can have some influence on the rate-dependent softening of the composite. The magnitude of the influence remains to be seen.

An important parameter in the development and application of the particle modified WBCs is the particle volume fraction $f$. A relatively large $f$ can lead to a very high flow stress at small strains and a very low flow stress at large strains compared with that of tungsten. The cost of this desired stress-strain behavior is the reduction of composite density, which is critical for kinetic energy penetrators. The optimal particle volume fraction is likely to depend on the velocity of the penetrator as well as the armor material; its identification falls out of the scope of the present study. However, the predictions for stress-strain behavior of the composite shown in Figs 13 and 14 can provide useful guidance for the initial selection of particle volume fraction.

Of the five controlling parameters studied, the radius $r$ of the particles has very little influence on the composite behavior if $r \leqslant 10$ $\mu$m. The particle volume fraction $f$ dictates the effects of both strengthening at small strains and thermal softening at large strains due to the glassy particles. The effects of the nondimensional parameters $\alpha$ and $\beta$ characterizing the thermal softening behavior of the particles are as follows: $\alpha$ affects the onset and the rate of thermal softening, while $\beta$ controls the transition strain range from non-softening to complete softening. The applied overall strain rate $\dot{\varepsilon}/\dot{\varepsilon}_0$ also affects both the onset and the rate of thermal softening: a large strain rate leads to an early onset and more abrupt thermal softening, while a small strain rate gives rise to the opposite. In general, owing to thermal softening of the glassy particles, the strain-rate sensitivity of the composite is reduced.

Considered in this study is the stress-strain behavior of a glass particle-modified tungsten-based composite (WBC) under uniaxial compression. However, during penetration, there is a high hydrostatic pressure present in the penetrator material due to lateral confinement. The effect of this hydrostatic compressive stress on thermal softening of the WBC is likely to be negligible, since the temperature increase in the WBC is owing to the plastic deformation of tungsten which is essentially independent of the hydrostatic pressure according to the $J_2$ flow theory (Hill, 1950).

In predicting the stress-strain behavior of the WBC, a few simplifications of the composite material have been made. For example, the "matrix" phase in a usual tungsten heavy alloy is excluded in the cell model; viscosity of the glass particles and thermal softening of the pure tungsten phase are neglected. These simplifications have allowed us to quantify the effect of thermal softening of the glass particles on the stress-strain behavior of the tungsten matrix composite. However, in order to predict the true behavior of the particle-modified tungsten-based composite, thermal softening of the pure tungsten phase and the "matrix" material (e.g., W-Ni-Fe) must be included in the model. Further, to validate the model predictions, the particle-modified WBC needs to be fabricated, and high strain rate experiments need to be performed. All of these studies are well under way, and the results will be reported subsequently.

*Acknowledgements*—This work was supported by the US Army Research Office under Award No. DAAH0494G0086 to G. Bao. Special thanks go to K. T. Ramesh for suggesting this modeling work to the authors. Helpful discussions with K. T. Ramesh and D. C. Nagle are gratefully acknowledged.

## REFERENCES

Anton, D. L. and Shah, D. M. (1994). High temperature ordered compounds for advanced aero-propulsion applications. In *High Temperature ordered Intermetallic Alloys III* (eds C. T. Liu *et al.*), Materials Research Society Symposium Proceedings, Vol. 133, pp. 361–367, Pittsburgh, PA.

Bao, G. (1996). High strain rate deformation of metals containing compressible and incompressible pores. To be published.

Bao, G., Hutchinson, J. W. and McMeeking, R. M. (1991). Particle reinforcement of ductile materials against plastic flow and creep. *Acta Metall. Mat.* **39**, 1871–1882.

Bao, G. and Lin, Z. (1996). High strain-rate deformation in particle reinforced metal matrix composites. *Acta Metall. Mat.* **44**, 1011–1019.

Bao, G. and Ramesh, K. T. (1993). Plastic flow of a tungsten-based composite under quasistatic compression. *Acta Metall. Mat.* **41**, 2711–2719.

Chin, E. S. C., Dowding, R. J. and Woolsey, P. (1993). Tungsten alloy penetrator interaction with a titanium aluminide composite. In *Proc. 1992 Conference on Tungsten and Tungsten Alloys*, MPIF, p. 497, Princeton, NJ.

Christensen, R. M. (1991). *Mechanics of Composite Materials*, Krieger Publishing Co., Malaber, FL, U.S.A.

Coates, R. S. and Ramesh, K. T. (1991). The rate-dependent deformation of a tungsten heavy alloy. *Mat. Sci. Engng* **A145,** 159–166.

Dunn, P. S. and Baker, B. D. (1993). Target penetration interaction: 70 volume percent tungsten-30 volume percent uranium penetrator material. In *Proc. 1992 Conference on Tungsten and Tungsten Alloys*. MPIF, p. 487. Princeton, NJ.

Fukuhara, M. and Abe, Y. (1993). High-temperature elastic moduli and internal friction of α-SiC ceramic. *J. Mat. Sci. Letters* **12,** 681–683.

German, R. M. (1993). Critical developments in tungsten heavy alloys. In *Proc. 1992 Conference on Tungsten and Tungsten Alloys*, p. 3. MPIF, Princeton, NJ.

Hill, R. (1950). *The Mathematical Theory of Plasticity*. Oxford University Press, Oxford, UK.

Hohler, V. and Stilp, A. J. (1990). Long-rod penetration mechanics. In *High Velocity Impact Dynamics* (ed. J. A. Zukas), p. 321. Wiley & Sons, New York, NY.

Lankford, J. (1992). High strain rate behavior of tungsten heavy alloys. In *High Strain Rate Behavior of Refractory Metals and Alloys* (eds R. Asfahani *et al.*), p. 267. TMS, Warrendale.

Magness, L. S. and Farrand, T. G. (1990). Deformation behavior and its relationship to the penetration performance of high-density KE penetrator materials. In *Proc. 1990 Army Science Conference*, p. 149. Durham, NC.

Magness, L. S. (1992a). Properties and performance of KE penetrator materials. In *Tungsten and Tungsten Alloys*, MPIF, p. 15. Princeton, NJ.

Magness, L. S. (1992b). A phenomenological investigation of the behavior of high-density materials under high pressure, high strain rate loading environment of ballistic impact. Ph.D. dissertation, The Johns Hopkins University.

Magness, L. S. (1994). High strain rate deformation behavior of kinetic energy penetrator materials during ballistic impact. *Mech. and Mat.* **19,** 147–154.

Nagle, D. C. (1995). Private communication.

Parker, E. (1967). *Material Data Book for Engineers and Scientists*, McGraw-Hill, New York.

Rabin, B. H. and German, R. M. (1988). Microstructure effects on tensile properties of tungsten-nickle-iron composites. *Metall. Trans. A* **19A,** 1523–1532.

Rall, K., Courtney, T. and Wulff, J. (1976). *Introduction to Material Science and Engineering*, Wiley, New York.

Ramesh, K. T. (1995). Private communication.

Shackelford, J. F. (1995). *The CRC Material Science and Engineering Handbook*, CRC Press, Boca Raton, FL.

Syre, R. (1965). *Handbook on the Properties of Niobium, Molybdenum, Tantalum, Tungsten and some of Their Alloys*, AGARDograph (NATO).

Zhou, M., Needleman, A. and Clifton, R. J. (1994). Finite element simulations of shear localization in plate impact. *J. Mech. Phys. Solids* **42,** 423–457.

Zurek, A. K., Follansbee, P. S. and Kapoor, D. (1992). Strain rate and temperature effects in tungsten and tungsten alloys. In *High Strain Rate Behavior of Refractory Metals and Alloys* (eds R. Asfahani, E. Chen and A. Crowson), TMS, pp. 179–192. Warrendale, PA.